EKSPLOATACJA I NIEZAWODNOŚĆ MAINTENANCE AND RELIABILITY

# Eksploatacja i Niezawodnosc – Maintenance and Reliability

**Volume 24 (2022), Issue 1**

journal homepage: http://www.ein.org.pl

Article citation info:
Breńkacz Ł, Bagiński P, Adamowicz M, Giziewski S. Failure analysis of a high-speed induction machine driven by a SiC-inverter and operating on a common shaft with a high-speed generator. Eksploatacja i Niezawodnosc – Maintenance and Reliability 2022; 24 (1): 177–185, http://doi.org/10.17531/ein.2022.1.20.

# Failure analysis of a high-speed induction machine driven by a SiC-inverter and operating on a common shaft with a high-speed generator

Indexed by: Web of Science Group

Łukasz Breńkacz[a,*], Paweł Bagiński[a], Marek Adamowicz[b], Sebastian Giziewski[c]

[a] Polish Academy of Sciences, Institute of Fluid Flow Machinery, ul. Fiszera 14, 80-231 Gdańsk, Poland
[b] Gdańsk University of Technology, Faculty of Electrical and Control Engineering, Gabriela Narutowicza 11/12, 80-233, Gdańsk, Poland
[c] SGI Engineering, MMB Drives Sp. z o.o., Maszynowa 26, 80-298 Gdańsk, Poland

## Highlights

- A numerical analysis of the failure of a high-speed turbomachine was performed.
- Run-out analysis was carried out after the failure was performed.
- Modifications to the design of a test rig for high-speed generators were analysed.
- Rolling bearings and their influence on rotor dynamics were analysed.

## Abstract

Due to ongoing research work, a prototype test rig for testing high speed motors/generators has been developed. Its design is quite unique as the two high speed machines share a single shaft with no support bearings between them. A very high maximum operating speed, up to 80,000 rpm, was required. Because of the need to minimise vibration during operation at very high rotational speeds, rolling bearings were used. To eliminate the influence of higher harmonics of supply voltage and current on the formation of torque oscillations on the shaft and excessive losses in the form of heat, a voltage source inverter with high switching silicon carbide (SiC) power transistors characterizing high precision of the output voltage generation with a fundamental harmonic frequency of several kilohertz has been used. During the first start-ups, it turned out that the system was not stable, and a failure occurred. The paper presents the consequences that may arise when a machine operating at a speed of about 70,000 rpm fails. The article contains pictures of a generator failure that occurred at a high rotational speed.

## Keywords

high-speed generator, failure analysis, rotor dynamics, rolling bearing.



## 1. Introduction

The last decade has seen a rapid development of high-speed electric drives, especially as regards their use in air turbo compressors for fuel cell systems [3], variable frequency drives for LNG pumps, vacuum pumps, machine tools, turning centres or specialised medical equipment. The same applies to power generation systems with high-speed electric generators and gas microturbines used in distributed generation [16, 17, 36].

The development of high-speed drives has been made possible by, among others: (i) the development of new-generation power electronic converters with fast silicon carbide (SiC) and gallium nitride (GaN) semiconductor devices that enable precise generation of sinusoidal voltages with fundamental harmonic frequencies of several kilohertz—while reducing the production cost of power electronic converters [8, 13, 23]; (ii) the improved efficiency of high-speed motors and generators [11, 16], which operate at speeds above 100,000 rpm [3, 17, 36]; (iii) improvements in bearing technology [36] and (iv) the development of high-speed digital signal processors (DSPs) for industrial applications—which enables the use of advanced control algorithms at high rotational speeds [12, 33]. The development of these technologies affects both high-speed induction motors/generators that are valued in the industry for their reliability, simple rotor design, low inertia, and ability to operate in high temperatures, as well high-speed permanent magnet motors/generators with high torque density and power density. The stator and rotor of a 3.4 kW generator and a 6-kW generator, which were used on the test rig analysed, are shown in Fig. 1.

The research and development of electric generators is the subject of interest in numerous scientific works. Basic information on permanent-magnet synchronous generators operating at high rotational speeds has been already presented by Arkkio et al. [4]. Design and analysis technologies of high-speed permanent magnet machines have been recently reviewed by Ismagilov et al. [14] and Liu et al. [21]. The mechanical characteristics of high-speed permanent-magnet synchronous generators with different shaft material with taking into account the overhang effect have been analyzed by Lee et al. [19]. A comprehensive sensitivity analysis of the rotor parameters on Multiphysics performance of the high-speed permanent magnet syn-

(*) Corresponding author.
E-mail addresses: Ł. Breńkacz (ORCID: 0000-0001-7480-9636): lukasz.brenkacz@imp.gda.pl, P. Bagiński (ORCID: 0000-0003-3753-7525): pbaginski@imp.gda.pl, M. Adamowicz (ORCID: 0000-0003-0561-8697): marek.adamowicz@pg.edu.pl, S. Giziewski (ORCID: 0000-0003-1197-0291): s.giziewski@gmail.com

*Fig. 1. Stator and rotor of a 3.4 kW induction motor/generator (left) and a 6-kW permanent magnet synchronous motor/generator (right) designed to operate at speeds above 80,000 rpm and voltage frequency above 1.3 kHz.*

chronous machine, including the electromagnetic properties, losses, rotor stress, rotor dynamics, and the temperature has been presented by Du et al. [10]. The influence of different rectifier topologies on a high-speed permanent magnet generator used in a micro-gas turbine distributed generation system has been studied by Qiu et al. [27]. The design criteria, assembly practices and experimental analysis of the whole low-cost micro generation system with a high-power density microturbine has been discussed by Pottie et al. [25] The investigation of dynamic properties of the microturbine with a maximum rotational speed of 120 krpm was shown by Żywica et al. [37]. The dynamic analysis of 1 kW, 30 kW, and 700 kW turbines were presented by Breńkacz et al. [5–7].

A summary of the current evolution of electric generators and their development trends are presented, for example, in the work by Antipov and Danilevich [2]. The authors examined high-speed electric generators in the speed range of 10,000 to 50,000 rpm. Generally, high speed generators have been the subject of a considerable number of studies, mainly of those dealing with their electrical properties. However, studies that focus on two generators simultaneously are far less common. An example of this is the work by Kuznetsov et al. devoted to the study of two generators [18]. In this study, the authors analysed the synchronisation of two generators.

Studies that focus on the diagnostics of generators can be found in the literature. An example of such a study can be found in the article by Skowronek and Woźniak [31]. To generator diagnostics, the authors proposed a new classification method used for failure analysis. They presented the characteristics of the method based on the alternator diode failures. This method was compared with other diagnostic methods. An analysis of the evolution of the online diagnostic method was presented by Rubanenko et al. [28]. The authors focused on synchronous generators. They created a fault tree of various components of synchronous generators. Identification of wear and failure of brake system components during the warranty service was presented by Sliż and Wycinka [32]. Monitoring and predicting bearing failure was presented by Castilla-Gutiérrez et al. [9]. An example of a computer analysis of disc brakes was presented by Pranta et al. [26]. The effect of rotor eccentricity on radial bearings was presented by Abdou and Saber [1]. The effect of rotor eccentricity on electrical and mechanical characteristics of different types of high-speed machines has been discussed by Lee and Hong [20]. Another approach, which is an online estimation of stator current harmonics for status monitoring and diagnosis of high-speed permanent magnet synchronous machines has been proposed by Lu et al. [24]. As stated in [24], obtaining the harmonic distribution and magnitudes can also provide a reliable reference for optimization in the motor design stage.

In power systems with gas microturbines, the microturbine disk and the high-speed generator rotor generally share a common shaft. The turbine is attached to the free end of the shaft and the rotor of the high-speed generator is in the central part of the shaft, between the two bearings. To achieve the highest possible torque density and power density, the generator stator is embedded in a steel casing with O-ring seals fitted at each end and then placed inside the outer casing of the cooling jacket. Cooling air flows through the air gap between the rotor and the stator to help cool the rotor and shaft, while a mixture of water and glycol is pumped through the cooling jacket to remove heat from the stator [16]. Two bearing hubs are located on the same shaft where the turbine disk and generator rotor are mounted.

At specific dimensions and speed of a high-speed generator, the power density obtained depends on the induction in the air gap and the current system provided by the flow of stator currents. When designing or selecting high-speed electric generators, the specifications for the air gap stresses obtained due to the magnetic field, as well as the restrictions on the cooling system, which provide the maximum values for the machine current system, must be observed. A particular challenge for maximising the heat removal capacity of the cooling system is to avoid or minimise heat losses other than those associated with current flow in the copper-plated stator winding.

In high-speed machines, the most important aspect is to ensure stable operation of the rotor over a wide range of rotational speeds. It is also particularly important to accurately predict the natural frequencies of the rotor during the design phase to minimise the likelihood of failure. Improper rotor design can lead to excessive acoustic noise emissions, accelerated wear, or even bearing damage. At high rotational speeds, the movement of rotating elements can cause mechanical resonance resulting in potential rotor failure or catastrophic contact with the stator.

There is currently no scientific article available that would present the dynamic properties of two generators mounted on a single shaft. There is also a lack of articles available that would show the damage of small high-speed generators. It is this gap that this article aims to fill.

## 2. Research object

A diagram of the test rig used for high-speed generators testing is shown in Fig. 2. The diagram shows the positions of the bearings, the generators, and the structure on which the stators of the two generators are placed. Generator 1 is an asynchronous motor (IM-mW5,4/6-2-52c/52cr9) [38]. Generator 2 is a synchronous motor (PMSM-mSpW 5.5/4.5 – 4 – a1) [39]. The length of the entire test rig is 288 mm, and its diameter is 130 mm. The O-ring seals and screws used to secure the various components of the casing are also visible on the structure. The radial clearance between the rotor and the stator of the first generator was 300 μm. This is the shortest distance between the rotating rotor and the structure. No strength or dynamic analysis were performed prior to designing and constructing this test rig.

Fig. 3 shows a model of the rotor with the generators, bearings and nuts providing pressure to the bearings. The bearing system comprises four rolling bearings. Two pairs of bearings are positioned at both ends of the rotor. The distance between the bearing pairs was 200 mm.

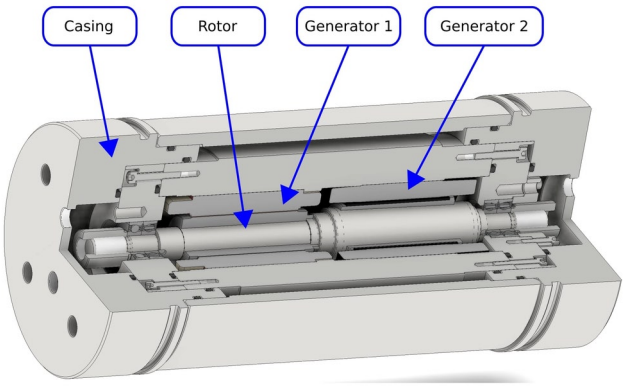


*Fig. 2. Diagram of the test rig used for testing high-speed generators*

The back-to-back arrangement, also known as the "O arrangement", was used for both pairs of bearings. To exert pressure on the bearings, two nuts were used at both ends of the shaft. High pressure was applied on the bearings (in compliance with the bearing manufacturer's catalogue [29]).

Four bearings marked with the designation HCB7001-C-2RSD-T-P4S were used in the design [29]. The acronym HCB indicates that these are hybrid bearings with ceramic balls. The meaning of individual bearing designation symbols used is as follows:

- "70" indicates that it is an average series
- "01" indicates that the inner diameter is 12 mm
- "P4S" is the standard FAG designation, which is higher than P4 according to the standard accuracies defined by DIN 620
- "T" indicates a laminated version with guidance on the outer ring
- "2RSD" indicates that the bearing is sealed on both sides and lubricated with grease
- "C" indicates that the bearing angle is 15 degrees.

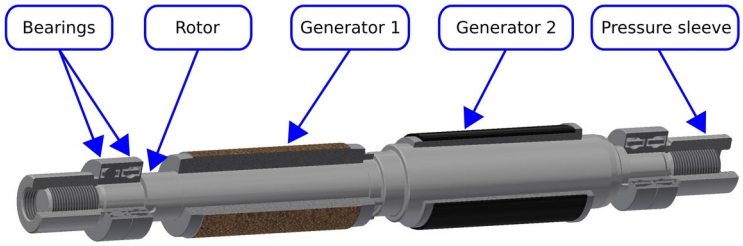


*Fig. 3. 3D model of the rotor*

The maximum speed permitted by the manufacturer for a single bearing is 85,000 rpm. The outer diameter of the bearing was 28 mm and its length was 8 mm.

To verify the performance of the high-speed generator system with a power electronic converter, it is advantageous to analyse the functioning of the generator on an experimental test rig using an additional high-speed motor that simulates the microturbine before mounting it on the target generation system with a gas microturbine [36].

On such a test rig, two high-speed machines are placed on a common shaft. While one acts as a drive motor modelling the changes in the shaft torque generated by the microturbine, the other is analysed at selected dynamic states and performance levels when generating electrical power.

The major challenges encountered when designing an advanced test rig for testing high-speed generators include meeting the test rig specifications, selecting bearings, and integrating them with the shaft of a high-speed generator and a high-speed motor that simulates the performance of a gas microturbine, designing and constructing a cooling system for the generator and motor, as well as designing and constructing a power electronic converter with a control system. It is also of major importance to comprehensively develop testing instruments, tools, and strategies to ensure testing on a component, subsystem and system level aimed at reducing the complexity and risk level when designing the target power system with a gas microturbine.

To run two high-speed machines with rotors embedded on a common shaft, it is necessary to examine the natural frequencies of the shaft by means of a simulation using the finite element method before operating the test rig [36]. In this analysis, the elasticity constant of the bearing system, which affects the rotational speed at which resonant vibrations occur, is considered. The length of the shaft is then adjusted so that the nominal speed remains between the second and third flexural vibration modes of the shaft [36].

When designing a power electronic converter feeding a motor in traditional industrial drives with voltage inverters, motor stator inductance is used to filter out higher-order harmonics from the inverter's output current. This helps to create a relatively smooth motor current waveform. Higher-order harmonics visible in the stator current waveforms result from the switching of the inverter transistors. Except for the first harmonic, the so-called "current ripples" appear in the motor current waveform, and their period corresponds to the switching period of the inverter transistors. The ripples that occur in the inverter current waveform do not affect torque generation; however, they cause hysteresis losses and losses due to eddy currents released as heat in the rotor and stator of the motor. The current components associated with high-frequency current ripples cause higher-order harmonics to appear in the magnetic flux waveform, which in turn induce voltages resulting in the flow of eddy currents in the rotor core and the stator core [35]. In synchronous motors with permanent magnets mounted on the surface of the rotor, the flow of eddy currents in the permanent magnets is also caused by the current ripples in the stator and the arrangement of the grooves. In particular, the increase in temperature of permanent magnets, which can lead to a deterioration of their magnetic properties, is a major problem. The existence of eddy currents requires the motor core to be made of thin sheet metal plates (25 μm thick), insulated on one side. Amorphous alloy sheets, for example, exhibit this property. Hysteresis losses, on the other hand, can be reduced by adding various additives to the ferromagnetic material, resulting in the smallest possible hysteresis loop width. Power losses due to hysteresis are proportional to frequency, and power losses due to eddy currents are proportional to the square of the frequency. In general, the losses associated with supplying the inverter using the voltage pulse-width modulation method increase exponentially with the switching frequency of the transistors and can be very large, even if the pulsed current does not appear to be large in relation to the amplitude of the fundamental harmonic [16].

High-speed motors, especially permanent magnet synchronous motors, are characterised by significantly lower inductance values of the stator winding compared to motors used in typical industrial applications. To reduce the losses of the power supply of the PWM (Pulse Width Modulation) inverter, especially in drives with permanent magnet synchronous motors/generators, it is necessary to use a sinusoidal filter, which must be placed between the inverter and the motor to ensure further reduction of current ripple beyond the damping capacity of the motor stator inductance. The resonant frequency of the sinusoidal filter must be significantly higher than the frequency of the fundamental harmonic of the motor voltage to avoid excessive losses in the drive, but also much lower than the switching frequency of the converter transistors to ensure sufficient filtering efficiency of ripple currents. The use of a sinusoidal filter mounted between the motor/generator and a typical two-level inverter causes a drop in the supply voltage of the high-speed motor and power losses in the filter itself. It also increases the price and the weight of the drive by the cost and the weight of the filter. Since voltage and current resonances can occur in an inverter system with a filter and a high-speed motor, resonance damping resistors are needed in addition to the sinusoidal filter.

The power losses in these components can be significant and this can reduce the efficiency of the inverter and the entire drive system by up to several per cent.

## 3. Methodology

In this study, we conducted experiments in laboratory conditions based on a specialized testbed with a digitally controlled power electronic converter and two investigated high-speed machines: high-speed induction motor and high-speed permanent magnet generator mounted on a common shaft. It was assumed that the high-speed induction motor driving the generator is supplied with sinusoidal voltage from a voltage inverter with SiC MOSFETs (Metal Oxide Semiconductor Field Effect Transistors).

Since the inverter itself is characterized by a square-wave output voltage with modulated square-wave pulse width, we used an LC filter to obtain a sinusoidal voltage at the output. Thus, the research assumed ideal conditions for supplying the generator with sinusoidal current, so that there was no significant influence of current harmonics on, for example, torque oscillations on the common shaft. Similarly, the research assumed ideal conditions for supplying the high-speed induction motor with sinusoidal voltage, so that there was no significant influence of the harmonics of the supply voltage on the excessive formation of losses and excessive heating of the investigated machine. The test stand prepared in such a way makes it possible to carry out tests of start-ups, speed changes and steady operation of the investigated high-speed machines while concentrating all efforts on examining the mechanical properties of machines in the conducted experiments.

Fig. 4 shows pictures of the designed power electronic converter with SiC transistors and an output sinusoidal filter feeding the high-speed motor that simulates the dynamic states of the gas microturbine on the test rig. To build the power electronic converter, the authors used silicon carbide semiconductor power devices such as SiC MOSFETs and SiC Schottky diodes. Commercially available SiC power devices can be used to increase both the efficiency and the control precision of power electronic converters suitable for use in the renewable energy applications, such as grid-connected photovoltaic (PV) generation systems, and in adjustable-speed electric drives, including high-speed drives with speeds above 100,000 rpm.

SiC MOSFETs have low conduction losses due to the low channel resistance between the drain and the source ($R_{DS(ON)}$) during conduction. For example, in the case of SiC MOSFETs (model C3M0021120K) used in the investigated test rig, the channel resistance $R_{DS(ON)}$ at a rated current of 74 A and at a temperature of 100°C amounts to 21 mΩ. SiC MOSFETs are controlled by a higher gate voltage (from –5 V to +20 V) than their silicon counterparts. They can be switched on and off much faster than IGBT (Insulated-Gate Bipolar Transistors) and have a higher operating frequency. Thanks to significantly lower switching losses, they enable the energy-efficient operation of PWM inverters at switching frequencies above 50 kHz.

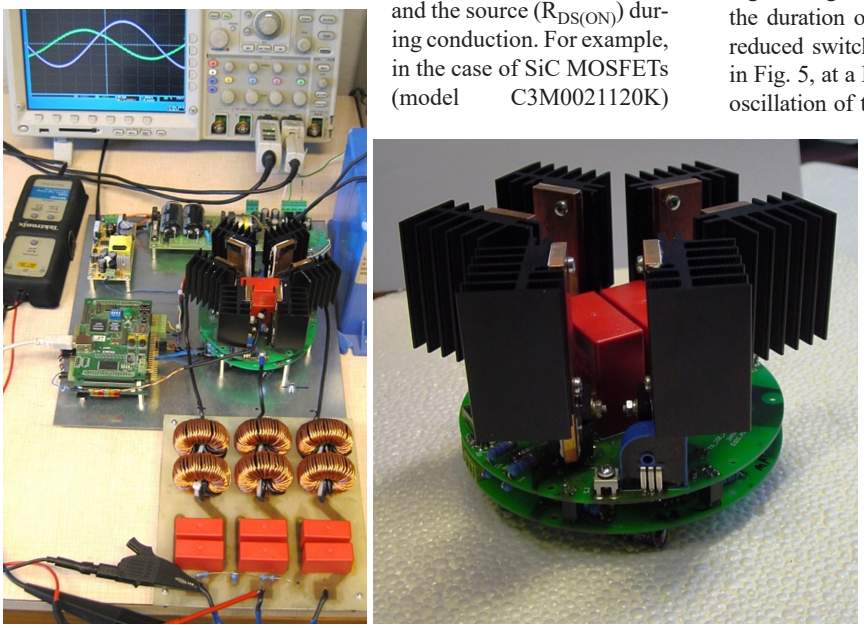

*Fig. 4. Pictures of the designed power electronic converter with SiC MOSFETs and sinusoidal output filter used to control the high-speed motor that simulates the dynamic states of the gas microturbine on the test rig*

The high switching frequency of SiC transistors, which allows voltage modulation frequencies higher than 50 kHz to be achieved, makes it possible to properly generate a voltage with a fundamental harmonic frequency significantly higher than that obtained in inverters with silicon IGBTs. According to [34], the voltage modulation factor is defined as follows:

$$m_f = f_{sw}/f_{1h} \tag{1}$$

where $f_{sw}$ stands for the voltage modulation frequency of the inverter and $f_{1h}$ stands for the frequency of the fundamental harmonic of the generated voltage; its value should be not less than 21. Therefore, to generate a voltage of 1,500 Hz, the inverter should operate with a modulation frequency of not less than $f_{sw} = 21 \cdot f_{1h} = 31.5$ kHz.

When switching voltages and currents within a very short time (in the range of nanoseconds), undesirable voltage and current oscillations may occur due to the existence of parasitic inductances and capacitances in high-current transistor switching circuits, as well as in transistor gate control circuits. High-frequency and high-amplitude oscillations can be a source of electromagnetic interference (EMI) and can cause serious problems with electromagnetic compatibility (EMC) [22]. As shown in Fig. 4, the voltage source inverter with SiC MOSFETs uses a circular main board with the DC-link capacitors located in the centre. This design was used to ensure that the distances between the SiC MOSFETs and the DC circuit terminals, which determine the parasitic inductance of the high-current circuit, are minimised and are the same for all six inverter transistors.

## 4. Results of experimental studies of a SiC inverter

Fig. 5 shows the voltage switching waveform of the C3M0021120K SiC MOSFET in the tested inverter. Due to the special design of the power circuit of the inverter and the SiC MOSFET gate driver, a very high voltage switching rate of 60 kV/µs has been achieved, reducing the duration of the switching process to tens of nanoseconds, which reduced switching losses. As can be seen from the waveform shown in Fig. 5, at a DC voltage of 670 V, the maximum value of the voltage oscillation of the SiC MOSFET transistor, which was obtained during the transient state of the voltage switching process, did not exceed 850 V, which is an acceptable value for a nominal transistor voltage of 1,200 V.

The parameters of the sinusoidal inductive – capacitive (LC) filter shown in Fig. 5 were selected assuming that the power electronic converter will be used to feed a 3.4 kW high-speed induction motor. The inductance of the filter (L) was calculated assuming that the permissible voltage drop (ΔU) of the inductor reactance is 10 V at a motor current ($I_n$) of 7 A and a frequency of the fundamental harmonic of the inverter voltage ($f_{1h}$) of 1,500 Hz, according to the following relation:

$$L = \frac{\Delta U}{2\pi f_{1h} I_n} \tag{2}$$

The capacitance (C) of the sinusoidal filter was chosen based on (3) and (4) so that the resonance frequency $f_{res}$ ($f_{res}$ – resonance frequency) of the filter would be 10 kHz:

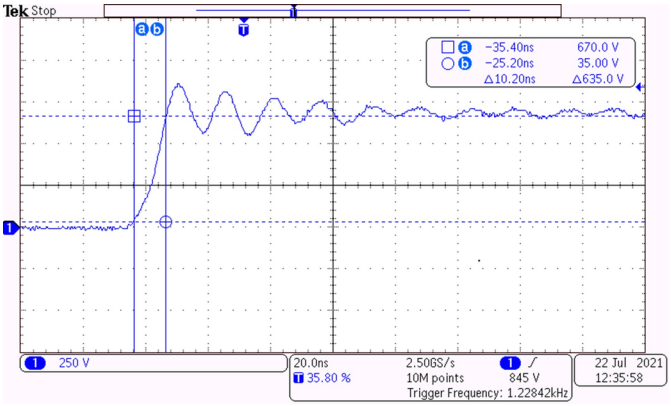


*Fig. 5. Voltage switching waveform of the SiC MOSFET transistor in the tested inverter*

$$f_{res} = \frac{1}{2\pi\sqrt{LC}} \tag{3}$$

$$C = \frac{1}{2\pi^2 f_{res}^2 L} \tag{4}$$

The modulation frequency $f_{sw}$ = 60 kHz has been selected. The inductance and capacitance values chosen for the sinusoidal filter are respectively 150 µH and 3 µF.

Fig. 6 shows the current and voltage oscillogram obtained at the output of the inverter. The high-frequency ripple currents visible on the current waveform have very high values (like the amplitude of the fundamental harmonic of the current) due to the very low inductance (about several millihenries) of the stator winding. Fig. 7 shows the current and voltage oscillogram obtained at the output of the sinusoidal filter in the tested system with a silicon carbide inverter.

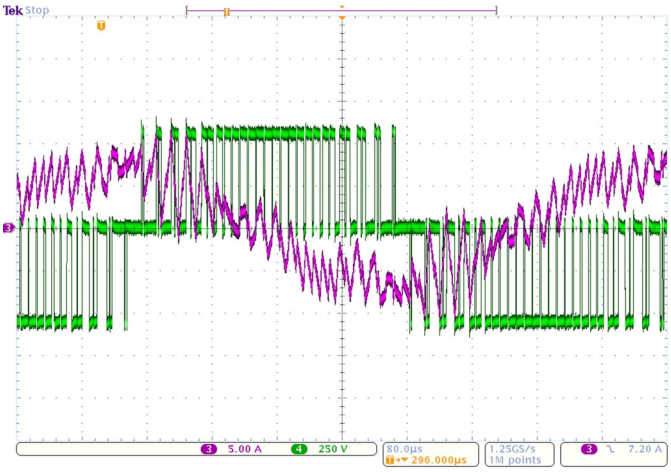


*Fig. 6. Voltage and current waveforms of the stator of a 3.4 kW induction motor installed in the tested system with a silicon carbide inverter at voltage frequency of 1.5 kHz measured before the sinusoidal filter*

Fig. 8 shows a comparison of the temperature increments of the stator of a 3.4 kW high-speed induction motor. The tests were performed at a motor load of 70% with the power supply at a voltage frequency of 1 kHz. Temperature measurements were carried out by measuring the resistance of a 4.7 kΩ negative temperature coefficient (NTC) thermistor mounted in the bearing disk of the high-speed induction motor. As shown in Fig. 8, the absence of a sinusoidal filter at the output of the inverter leads to an abrupt and very large increase in the temperature of the stator due to thermal losses caused by eddy currents and hysteresis losses in the stator core. The use of the LC


*Fig. 7. Voltage and current waveforms of the stator of a 3.4 kW induction motor installed in the tested system with a silicon carbide inverter measured after the sinusoidal filter at a voltage frequency of 1.5 kHz*

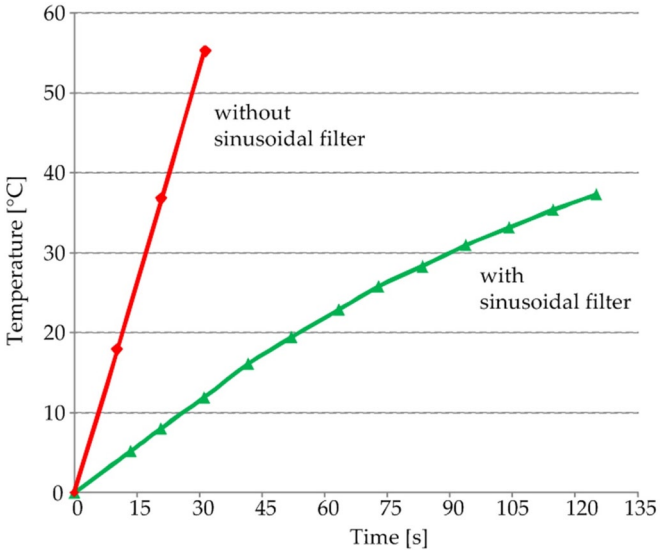


*Fig. 8. Temperature increments of the stator of a 3.4 kW high-speed induction motor powered by a SiC inverter with and without a sinusoidal filter*

sinusoidal filter results in a significant reduction of thermal losses and allows the high-speed motor to run for a long time.

## 4. Failure analysis

After the construction of the test rig, its operation was stable at low speeds of several tens of thousands of revolutions per minute. However, when approaching the nominal speed (after reaching a speed of about 60,000 rpm), it suffered damage visible in Fig. 9. In the first generator, located on the left, the distance between the rotor and the stator was only 300 µm. Due to the increased vibration amplitude, there was contact between the rotor and the stator. There is a scratch at the point of contact occupying a good portion of the generator.

Fig. 10 shows a zoom-in on the damaged rotor. The upper part of this figure, a), shows the generator attached to the shaft and the lower part, b), shows the generator removed from the shaft. The damage caused by the failure does not occupy the entire circumference of the generator; it is only local damage. Cavities of about 0.3 mm in depth are visible. This damage occupies approximately 1/3 of the circumference of the generator and 1/2 of its length. Dark discolourations can be seen around the cavities, which occurred due to the increase in temperature caused by friction and an electrical short circuit.



*Fig. 9. Damaged rotor*

*Fig. 9. Damaged rotor*

a)

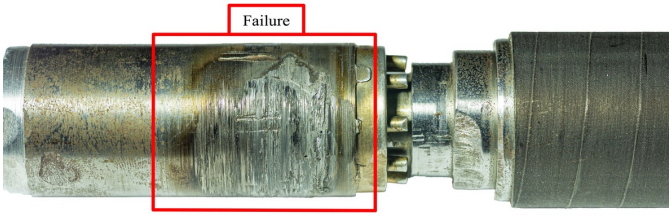


b)

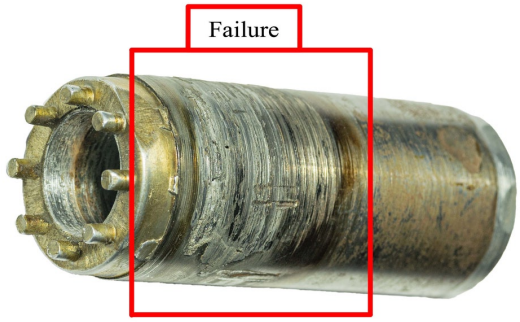


*Fig. 10. Pictures showing a) a zoom-in on the damaged generator attached to the shaft, b) damaged generator. The damage is inside red rectangles*

*Table 1. Summary of run-out measurements measured in seven planes*

| Angle | Plane 1 | Plane 2 | Plane 3 | Plane 4 | Plane 5 | Plane 6 | Plane 7 |
|---|---|---|---|---|---|---|---|
| 0 | 0.000 | 0.005 | 0.006 | 0.010 | 0.032 | 0.019 | 0.000 |
| 45 | 0.000 | -0.004 | 0.034 | 0.015 | 0.031 | 0.019 | 0.000 |
| 90 | 0.000 | 0.018 | 0.035 | 0.020 | 0.032 | 0.020 | 0.000 |
| 135 | 0.000 | 0.059 | 0.094 | 0.021 | 0.034 | 0.022 | 0.000 |
| 180 | 0.000 | 0.093 | 0.133 | 0.021 | 0.035 | 0.031 | 0.000 |
| 225 | 0.000 | 0.116 | 1.135 | 0.013 | 0.036 | 0.026 | 0.000 |
| 270 | 0.000 | 0.100 | 0.070 | 0.000 | 0.036 | 0.023 | 0.000 |
| 315 | 0.000 | 0.056 | 0.029 | 0.004 | 0.036 | 0.022 | 0.000 |
| 360 | 0.000 | 0.005 | 0.019 | 0.010 | 0.036 | 0.019 | 0.000 |

As part of the analysis of the damaged rotor, run-out measurements were carried out using a dial gauge with a measurement accuracy of one hundredth of a millimetre. These measurements are summarised in Table 1. A graphical representation of the shaft geometry is shown in Fig. 11. Some planes are not visible because they are too small in comparison with the planes with the highest displacements.

## 5. Numerical model

A numerical model was created using MADYN 2000 software to analyse the strength and dynamic properties [30]. A graphical representation of the beam model, with its dimensions and bearing positions, is shown in Fig. 12. This model consisted of 34 beam elements. The rotor mass was 0.987 kg, and the total length of the shaft was 261 mm. These values are the same as those of the manufactured rotor. The bearings were placed at nodes 6, 8, 28 and 30. The axial stiffness of each bearing was 31.1 N/µm and the radial stiffness was 186.6 N/µm. The damping was assumed to be 100 N·s/m for each bearing direction. Steel having the following parameters was selected as the material for the rotor:

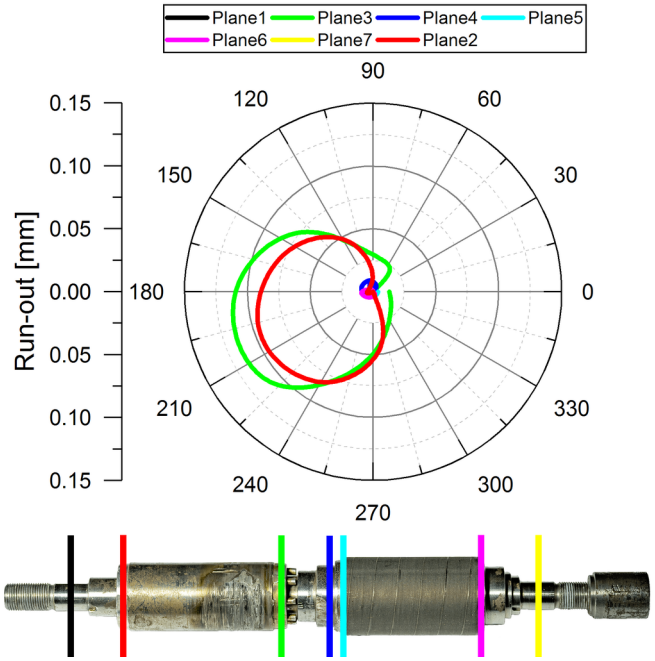


*Fig. 11. Shaft run-out analysis*

- Young's modulus – 205,900 MPa,
- Poisson ratio – 0.3,
- Density – 7,850 kg/m$^3$.

The generators were modelled as disks with an inner diameter equal to the diameter of the rotor. The inner diameter of the first and second generator was 29.4 mm and 31 mm, respectively. The generators were modelled using copper with the following parameters:

- Young's modulus – 100,000 MPa,
- Poisson ratio – 0.3,
- Density – 7,000 kg/m$^3$.

The unbalance is shown schematically in Fig. 13. For a balance quality grade of G2.5, a rotor mass of 0.912 kg and a speed of 80,000 rpm, the

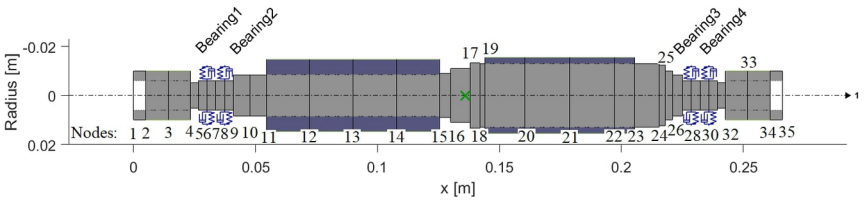


*Fig. 12. Beam model*

unbalance permitted according to the ISO 1940 standard [15] is 0.294 g·mm. It was placed at node 17.

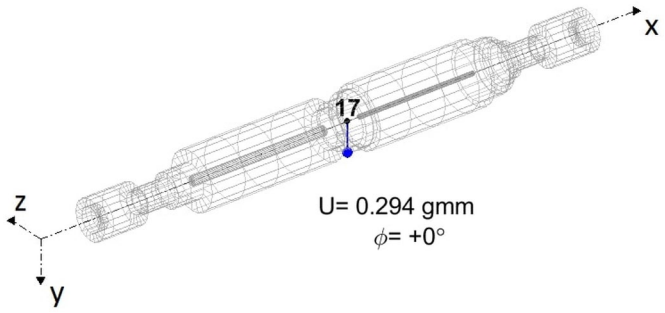


*Fig. 13. Rotor unbalance*

## 6. Results of numerical analyses

For the static analyses, the only force acting on the rotor was assumed to be the gravity of 9.81 m/s$^2$ acting along Y-axis. The displacement results are shown in Fig. 14. The static deflection of the rotor has the highest value in its central part, where it amounts to approximately 0.3 µm.

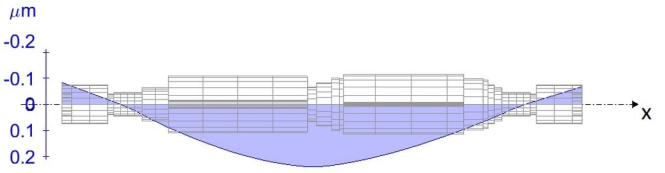


*Fig. 14. Displacements due to gravity*

The results of the reduced stresses due to the gravitational force are shown in Fig. 15. The maximum reduced stress did not exceed 0.5 MPa. The forces in the bearings are about 5 N and the bending moment reaches a maximum value of 0.2 Nm in the central part of the rotor. All the values of displacements, forces, moments, and stresses were found to be significantly lower than those allowed for this type of design.

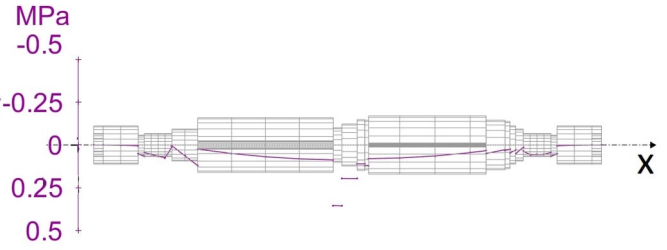


*Fig. 15. Reduced stresses*

When a rotor is in operation, one of the greatest risks is the occurrence of resonances at nominal speeds or when starting the machine. It is also important that the sub synchronous and super synchronous vibrations (induced for example by a clutch) do not coincide with the resonant frequencies. After the modal analysis, the first bending mode of natural vibrations (shown in Fig. 16) was found to occur at a frequency of 1,127.23 Hz, which corresponds to a speed of 67,633.6 rpm. The first bending mode of natural vibrations occurs at a speed dangerously close to the originally planned nominal speed.

To check whether the unbalance can induce natural vibration of the structure, a harmonic analysis must be performed. The results of the forced vibration analysis are shown in Fig. 17. The green line on the graph represents the vibration amplitude of the journal of the first bearing as a function of speed from 0 to 160,000 rpm. The red line, on the other hand, represents the vibration amplitude of node No. 15 in the central part of the rotor. This is the last node of the first generator and thus the part of the rotor that is most vulnerable to abrasion. For

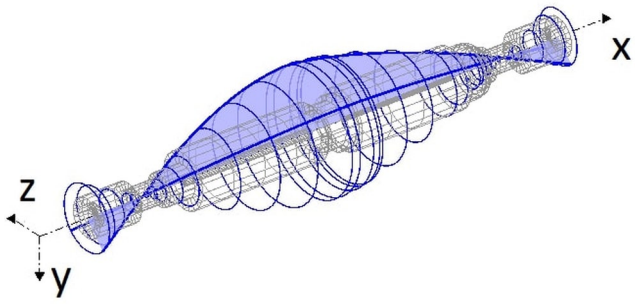


*Fig. 16. The first form of natural vibrations of the rotor*

design reasons, the distance between the rotor and the stator in this area, measured radially, is only 300 µm. In the numerical model, the global damping was assumed to be 1%. The blue vertical line indicates the nominal rotational speed. The maximum vibration amplitude occurred at a speed of 67,277 rpm and was 0.56 µm at the bearing journal and 26.33 µm at the central part of the rotor.

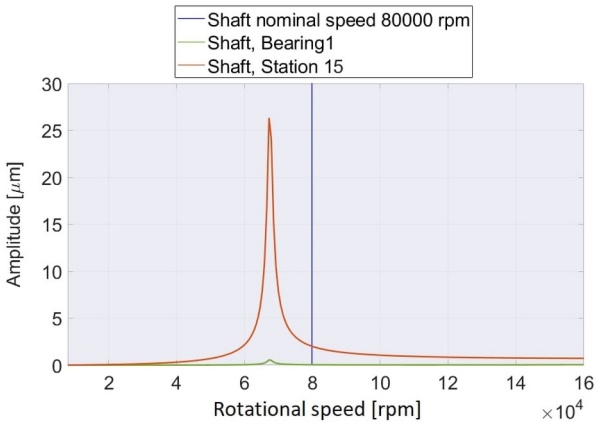


*Fig. 17. Forced vibration analysis*

## 7. Analysis of the causes of failure and proposals for changes

After carrying out several preliminary analyses, it became apparent that several factors contributed to the damage to the test rig analysed. Most importantly, the rotor was designed in such a way that the first bending mode of natural vibrations was in the expected speed range. This bending mode occurred at a speed of 67,277 rpm, whilst the nominal speed was designed to be equal to 80,000 rpm. The second very important factor was the presence of whipping between the rotor and the first generator (which occurred even before the rotor was damaged). The third and final factor was the selection of bearings that could operate at speeds of up to 85,000 rpm for a single bearing (according to the manufacturer's catalogue). However, no consideration was given to the fact that when a set of four bearings is in operation and the preload is high, the maximum speed should be reduced by a factor of 0.57, meaning that the bearings can only operate safely up to a speed of 48,450 rpm. Since the structure is not able to sustain large forces and moments, a set of four bearings is also not necessary. As part of the study, the geometry of the rotor was suggested to be changed so that the first bending mode of natural vibrations could be present at a higher rotational speed. A proposal was also made to change the type of bearings used. By changing the type of bearings, the permitted speed would be increased.

To increase the resonant speed of the rotor, a change in geometry was proposed which would increase the stiffness of the rotor. The new geometry is shown in Fig. 18. The updated model comprised 26 beam elements (8 fewer elements). The central beam element was shortened by 5 mm. After the modification, the model's weight was 0.897 kg, i.e., 15 grams lighter. The shaft had an overall length of 223 mm,

making it 38 millimetres shorter. The bearings were placed at nodes 5 and 23.

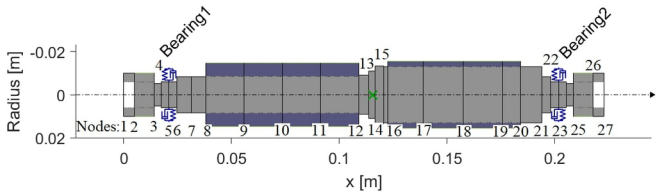


*Fig. 18. Beam model*

A different type of hybrid bearing with ceramic balls, designated HCB7000-C-2RSD-T-P4S, was used than before. The meaning of individual bearing designation symbols used is as follows:

- "70" indicates that it is an average series,
- "00" indicates that the inner diameter is 10 mm,
- "P4S" is the standard FAG designation, which is higher than P4 according to the standard accuracies defined by DIN 620,
- "T" indicates a laminated version with guidance on the outer ring,
- "C" indicates that the bearing angle is 15 degrees,
- "2RSD" indicates that the bearing is sealed on both sides and lubricated with grease.

The maximum speed permitted by the manufacturer for a single bearing is 95,000 rpm. A speed ratio of 0.75 must also be considered when using a two-bearing system with average tension. The maximum speed permitted by the manufacturer for these bearings is 71,250 rpm. This is lower than the previously assumed speed of 80,000 rpm. However, such a high speed is impossible to achieve anyway due to the resonant speed (as confirmed by the analyses below). The outer diameter of the bearing was 26 mm, and its length was 8 mm. At average bearing tension, the axial stiffness of each bearing was 18.5 N/µm, while the radial stiffness was 111 N/µm.

The unbalance was placed at node 14. As the shaft mass was changed to 0.912 kg, the permissible unbalance value, according to the ISO 1940 standard and a balance quality grade of G2.5, was now equal to 0.272 g·mm and the unbalance was placed at the centre of the rotor, i.e., at node 14.

The forced vibration analysis shows (Fig. 19) that the maximum displacement of the bearing journal (node 5 – green line) and of the part of the rotor which is most exposed to stator rubbing (node 12 – red line) was respectively 3.97 µm and 26.76 µm at a speed of 72,130 rpm. Compared to the reference case, the vibration amplitude has hardly changed. What has changed is the speed at which the resonant vibration occurred; it changed by 4,853 rpm. This indicates an increase in the maximum permissible speed of almost 5,000 rpm. However, for safety reasons, a speed of 6,000 rpm should not be exceeded.

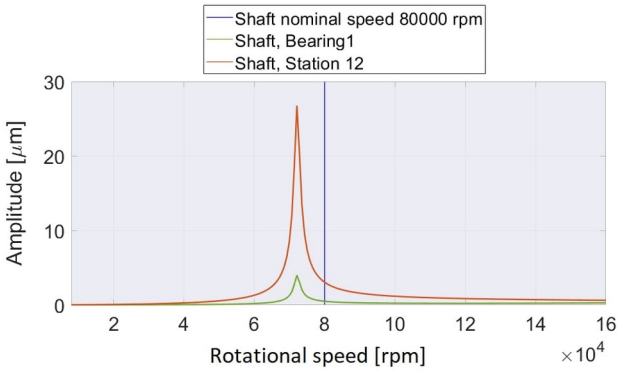


*Fig. 19. Forced vibration analysis*

## 9. Summary and conclusions

In this study, the dynamic properties of a test rig used to examine two generators were analysed. After it was designed and built, it was found to have failed. The paper presents the causes and consequences of such a failure. Several reasons contributed to its appearance. It turned out that the required speed of 80,000 rpm could not be achieved due to a resonance occurring at a speed of 67,277 rpm. The bearings were poorly selected, preventing them from operating at the higher speeds expected; and safe operation was only possible up to a speed of 48,450 rpm. There were also manufacturing errors encountered associated with whipping. Although the machine was balanced using an appropriate balance quality grade (G2.5), a failure occurred at a speed of about 60,000 rpm. This failure was most likely caused by the bearings operating at a speed greater than the maximum speed allowed by the manufacturer.

After the design was analysed, a change in the geometry of the rotating system was suggested to ensure that the first bending mode of natural vibrations does not occur until a speed of 72,130 rpm is reached. After the modifications, the first bending mode of natural vibrations will be excited at a speed that is 4,853 rpm higher than in the original design. After analysis, it became clear that without an additional support bearing located in the central part of the rotor—which, for design reasons, would involve two additional bearings and a coupling—operation at the originally planned speed of 80,000 rpm would not be possible. The maximum permissible speed after modifications would be equal to 60,000 rpm. The other way to increase the rotational speed is to use different types of bearings for example gas bearings, gas-foil bearings, or active foil bearings.

***Acknowledgements***

*This paper was created within the framework of the ACTIVERING project entitled "Active foil bearings with variable dynamic properties", agreement no. LIDER/51/0200/L9/17/NCBR/2018, which is being implemented as part of the research and development programme called "LEADER".*

*The research was conducted using equipment from the KEZO research centre in Jablonna.*

*The calculations were performed using computers from the IT Centre of the Tri-city Academic Computer Network.*

## References

1. Abdou KM, Saber E. Effect of rotor misalignment on stability of journal bearings with finite width. Alexandria Engineering Journal 2020; 59(5): 3407–3417, https://doi.org/10.1016/j.aej.2020.05.020.
2. Antipov VN, Danilevich YB. High-speed electrical machines for power engineering: Current state and development trends. Russian Electrical Engineering 2007; 78(6): 277–279, https://doi.org/10.3103/S1068371207060016.
3. Antivachis M, Dietz F, Zwyssig C et al. Novel high-speed turbo compressor with integrated inverter for fuel cell air supply. Frontiers in Mechanical Engineering 2021; 6(February): 1–13, https://doi.org/10.3389/fmech.2020.612301.
4. Arkkio A, Jokinen T, Lantto E. Induction and permanent-magnet synchronous machines for high-speed applications. 2005 International Conference on Electrical Machines and Systems, IEEE: 2005: 871–876, https://doi.org/10.1109/ICEMS.2005.202668.
5. Breńkacz Ł, Żywica G, Bogulicz M. Selection of the Bearing System for a 1 kW ORC Microturbine. Mechanisms and Machine Science, 2019; 60: 223–235, https://doi.org/10.1007/978-3-319-99262-4_16.

6. Breńkacz Ł, Żywica G, Bogulicz M. Numerical Analysis of the Rotor of a 30 kW ORC Microturbine Considering Properties of Aerodynamic Gas Bearings. Mechanics and Mechanical Engineering 2018; 22(2): 425–436, https://doi.org/10.2478/mme-2018-0034.
7. Breńkacz Ł, Żywica G, Bogulicz M. Analysis of dynamical properties of a 700 kW turbine rotor designed to operate in an ORC installation. Diagnostyka 2016; 17(2): 17–23.
8. Carpenter AL, Beechner TL, Tews BE, Yelvington PE. Hybrid-electric turbocharger and high-speed SiC variable-frequency drive using sensorless control algorithm. Journal of Engineering for Gas Turbines and Power 2018; 140(12): 1–8, https://doi.org/10.1115/1.4040012.
9. Castilla-Gutiérrez J, Fortes Garrido JC, Davila Martín JM, Grande Gil JA. Evaluation procedure for blowing machine monitoring and predicting bearing skfnu6322 failure by power spectral density. Eksploatacja i Niezawodnosc - Maintenance and Reliability 2021; 23(3): 522–529, https://doi.org/10.17531/ein.2021.3.13.
10. Du G, Huang N, Zhao Y et al. Comprehensive Sensitivity Analysis and Multiphysics Optimization of the Rotor for a High Speed Permanent Magnet Machine. IEEE Transactions on Energy Conversion 2021; 36(1): 358–367, https://doi.org/10.1109/TEC.2020.3005568.
11. Gerlach ME, Zajonc M, Ponick B. Mechanical stress and deformation in the rotors of a high-speed PMSM and IM. Elektrotechnik und Informationstechnik 2021; 138(2): 96–109, https://doi.org/10.1007/s00502-021-00866-5.
12. Giziewski S. Trójfazowy falownik napięcia z tranzystorami SiC JFET. Przegląd Elektrotechniczny 2012; 88(4b): 76–79.
13. He J, Li C, Jassal A et al. Multi-domain design optimization of dv/dt filter for SiC-based three-phase inverters in high-frequency motor-drive applications. IEEE Transactions on Industry Applications 2019; 55(5): 5214–5222, https://doi.org/10.1109/TIA.2019.2922306.
14. Ismagilov FR, Uzhegov N, Vavilov VE et al. Multidisciplinary Design of Ultra-High-Speed Electrical Machines. IEEE Transactions on Energy Conversion 2018; 33(3): 1203–1212, https://doi.org/10.1109/TEC.2018.2803146.
15. iso.org. ISO 1940-1:2003 Mechanical vibration - balance quality requirements for rotors in a constant (rigid) state. Part 1: Specification and verification of balance tolerances. 2003: 1–28.
16. Kim D, O'Connor J, Schwenne F, Drumm M. Design and test of an advanced system for energy generation. 2020.
17. Krähenbühl D, Zwyssig C, Bitterli K et al. Evaluation of ultra-compact rectifiers for low power, high-speed, permanent-magnet generators. IECON Proceedings Industrial Electronics Conference 2009; (Cm): 448–455, https://doi.org/10.1109/IECON.2009.5414964.
18. Kuznetsov AP, Stankevich NV, Shchegoleva NA. Synchronization of coupled generators of quasi-periodic oscillations upon destruction of invariant curve. Izvestiya Vysshikh Uchebnykh Zavedeniy. Prikladnaya Nelineynaya Dinamika 2021; 29(1): 136–159, https://doi.org/10.18500/0869-6632-2021-29-1-136-159.
19. Lee J I, Bang TK, Lee HK et al. Design of the high-speed pmsg with two different shaft material considering overhang effect and mechanical characteristics. Applied Sciences (Switzerland) 2021; 11(16): 0–8, https://doi.org/10.3390/app11167670.
20. Lee TW, Hong DK. Electrical and mechanical characteristics of a high-speed motor for electric turbochargers in relation to eccentricity. Energies 2021. doi:10.3390/en14113340, https://doi.org/10.3390/en14113340.
21. Liu L, Guo Y, Lei G, Zhu J. Design and Analysis Technologies of High Speed Permanent Magnet Machines. 2021 31st Australasian Universities Power Engineering Conference (AUPEC), 2021: 1–6, https://doi.org/10.1109/AUPEC52110.2021.9597696.
22. Liu T, Wong TTY, Shen ZJ. A survey on switching oscillations in power converters. IEEE Journal of Emerging and Selected Topics in Power Electronics 2020; 8(1): 893–908, https://doi.org/10.1109/JESTPE.2019.2897764.
23. Loncarski J, Monopoli VG, Leuzzi R et al. Analytical and simulation fair comparison of three level Si IGBT based NPC topologies and two level SiC MOSFET based topology for high speed drives. Energies 2019; 12(23): 1–16, https://doi.org/10.3390/en12234571.
24. Lu Y, Zhang X, Zhu C et al. On-line Estimation of Current Harmonics for Status Monitoring and Diagnosis of High-Speed Permanent Magnet Synchronous Motors. 2021 IEEE International Conference on Mechatronics (ICM), 2021: 1–6, https://doi.org/10.1109/ICM46511.2021.9385654.
25. Pottie DLF, Mendonça GA, Faria OA et al. Some aspects of the electromechanical design of high-speed microturbines for power generation. International Journal of Applied Electromagnetics and Mechanics 2020; 63(4): 621–644, https://doi.org/10.3233/JAE-190166.
26. Pranta MH, Rabbi MS, Banik SC et al. A computational study on structural and thermal behavior of modified disk brake rotors. Alexandria Engineering Journal 2021, https://doi.org/10.1016/j.aej.2021.07.013.
27. Qiu H, Zhao X, Wei Y et al. Comparative analysis of super high-speed permanent magnet generator electromagnetic and temperature fields with the PWM and uncontrolled rectifiers. EPE Journal 2020; 30(4): 181–191, https://doi.org/10.1080/09398368.2020.1776494.
28. Rubanenko O, Gundebommu S L, Hunko I, Peroutka Z. Analysis of development directions of online diagnostics of synchronous generator. Przegląd Elektrotechniczny 2021; 1(4): 22–28, https://doi.org/10.15199/48.2021.04.04.
29. Schaeffler. Super precision bearings. 2019: 262.
30. Schmied J, Perucchi M, Pradetto J C. Application of madyn 2000 to rotordynamic problems of industrial machinery. Proceedings of the ASME Turbo Expo 2007; 5(November): 799–810, https://doi.org/10.1115/GT2007-27302.
31. Skowronek K. FFT-PCA-LDA classifier in A.C . generator diagnostics. Eksploatacja i Niezawodnosc – Maintenance and Reliability 2013; 15(2): 140–146.
32. Sliż P, Wycinka E. Identification of factors that differentiate motor vehicles that have experienced wear or failure of brake system components during the warranty service period. Eksploatacja i Niezawodnosc 2021; 23(3): 430–442, https://doi.org/10.17531/EIN.2021.3.4.
33. Stumpf P, Bara I. Model predictive torque control with synchronized sampling frequency for high frequency induction machine drives. IEEE International Symposium on Industrial Electronics 2020; 2020-June: 332–338, https://doi.org/10.1109/ISIE45063.2020.9152245.
34. Stumpf P, Varga Z, Bartal P et al. Effect of subharmonics on the operation of ultrahigh speed induction machines. IECON Proceedings Industrial Electronics Conference 2009: 426–431, https://doi.org/10.1109/IECON.2009.5414960.
35. Zhang C, Chen L, Wang X, Tang R. Loss calculation and thermal analysis for high-speed permanent magnet synchronous machines. IEEE Access 2020; 8: 92627–92636, https://doi.org/10.1109/ACCESS.2020.2994754.
36. Zwyssig C, Kolar J W, Thaler W, Vohrer M. Design of a 100 W, 500000 rpm permanent-magnet generator for mesoscale gas turbines. Conference Record - IAS Annual Meeting IEEE Industry Applications Society 2005; 1(Im): 253–260, https://doi.org/10.1109/IAS.2005.1518318.
37. Żywica G, Kaczmarczyk T Z, Breńkacz Ł et al. Investigation of dynamic properties of the microturbine with a maximum rotational speed of 120 krpm – predictions and experimental tests. Journal of Vibroengineering 2020; 22(2): 298–312, https://doi.org/10.21595/jve.2019.20816.
38. Asynchronous motor mW 5.4/6-2-52c/52cr9 data sheet. e+a Elektromaschinen und Antriebe AG, 2010.
39. Synchronous motor mSpW 5.5/ 4.5-4-a1 ENCA data sheet. e+a Elektromaschinen und Antriebe AG, 2010.